AFRL-IF-RS-TR-2004-38
Final Technical Report
February 2004

OPTICAL PROPERTIES OF BOUND ANTIGEN MONOLAYERS FOR BIOMOLECULAR MICROSENSORS

University of California at Santa Barbara

Sponsored by
Defense Advanced Research Projects Agency
DARPA Order No. E117

AIR FORCE RESEARCH LABORATORY
INFORMATION DIRECTORATE
ROME RESEARCH SITE
ROME, NEW YORK

STINFO FINAL REPORT

This report has been reviewed by the Air Force Research Laboratory, Information Directorate, Public Affairs Office (IFOIPA) and is releasable to the National Technical Information Service (NTIS). At NTIS it will be releasable to the general public, including foreign nations.

AFRL-IF-RS-TR-2004-38 has been reviewed and is approved for publication.

APPROVED: /s/

DANIEL J. BURNS
Project Engineer

FOR THE DIRECTOR: /s/

JAMES A. COLLINS, Acting Chief
Information Technology Division
Information Directorate

REPORT DOCUMENTATION PAGE

Form Approved
OMB No. 074-0188

1. AGENCY USE ONLY (Leave blank)	2. REPORT DATE	3. REPORT TYPE AND DATES COVERED
	FEBRUARY 2004	Final Aug 01 – Sep 03

4. TITLE AND SUBTITLE
OPTICAL PROPERTIES OF BOUND ANTIGEN MONOLAYERS FOR BIOMOLECULAR MICROSENSORS

5. FUNDING NUMBERS
C - F30602-01-2-0538
PE - 61101E
PR - E117
TA - 00
WU - 67

6. AUTHOR(S)
Daniel A. Cohen

7. PERFORMING ORGANIZATION NAME(S) AND ADDRESS(ES)
University of California at Santa Barbara
Department of Electrical and Computer Engineering
Santa Barbara California 93106

8. PERFORMING ORGANIZATION REPORT NUMBER
N/A

9. SPONSORING / MONITORING AGENCY NAME(S) AND ADDRESS(ES)
Defense Advanced Research Projects Agency
3701 North Fairfax Drive
Arlington Virginia 22203-1714

AFRL/IFTC
26 Electronic Parkway
Rome New York 13441-4514

10. SPONSORING / MONITORING AGENCY REPORT NUMBER
AFRL-IF-RS-TR-2004-38

11. SUPPLEMENTARY NOTES
AFRL Project Engineer: Daniel J. Burns/IFTC/(315) 330-2335/ Daniel.Burns@rl.af.mil

12a. DISTRIBUTION / AVAILABILITY STATEMENT
APPROVED FOR PUBLIC RELEASE; DISTRIBUTION UNLIMITED.

12b. DISTRIBUTION CODE

13. ABSTRACT ***(Maximum 200 Words)***
The formalism of molar refraction was extended to cover the wavelength range of 200 nm - 2500 nm, in order to predict the index of refraction and index increment of a wide range of molecules of biochemical interest. Data for the model was obtained using a unique interferometer cell within a standard laboratory spectrophotometer. The resulting models for protein index increment suggest that both the sensitivity and specificity of refractometric sensors may be improved by operating at ultraviolet wavelengths and that measurement at two wavelengths may be used to quantify the total protein present and distinguish between similar proteins, of potential use to reduce false positive responses in affinity assays. The impact of refractive index and particle size on semiconductor-based evanescent field sensors was analyzed, along with the magnitude of optical scattering. The results are particularly important in quantitatively explaining the benefits of using a nanoparticle-enhanced assay, and of using high-index nanoparticles for enhancement. For particles below 100 nm in diameter, optical scattering will be negligible. For particles larger than 100 nm, scattering becomes measurable, and single one-micron diameter particles were detected in a novel monolithic evanescent field sensor.

14. SUBJECT TERMS
Biochemical Sensors, Optical Sensors, Optical Properties, Optoelectronics

15. NUMBER OF PAGES
26

16. PRICE CODE

17. SECURITY CLASSIFICATION OF REPORT	18. SECURITY CLASSIFICATION OF THIS PAGE	19. SECURITY CLASSIFICATION OF ABSTRACT	20. LIMITATION OF ABSTRACT
UNCLASSIFIED	UNCLASSIFIED	UNCLASSIFIED	UL

Table of Contents

List of Figures

1. Introduction and Goals

Optical methods provide the highest sensitivity for the detection and measurement of biochemical species, and concerted effort is underway worldwide to transfer laboratory techniques to industrial, clinical, and battlefield settings. These applications will benefit greatly by miniaturizing the sensor and integrating it directly with microelectronics, and the resulting "laboratory on a chip" will have greatly improved speed, sensitivity, reliability, size, and cost. Optical techniques that have been successful include evanescent field excitation of fluorescence, surface plasmon resonance and microcavity resonance, evanescent field absorption, monochromatic or white light interferometry, and intracavity laser refractometry. In all of these cases, the measurement depends on the interaction of the optical field with both the analyte and the medium in which it is carried. Knowledge of the optical constants of the analyte is crucial to the interpretation of the results, as well as modeling new measurement systems. However, the optical constants have not been measured in a systematic way, and the scarce data that exists is scattered through decades of literature, and often buried in reports that an engineer in photonics will find difficult to understand. Thus, the goal of this work was to determine the optical properties of biomolecules relevant to advanced microsensors, and to model the impact that these optical properties have on microsensor performance. Of particular interest were the spectrally resolved index of refraction, absorption, and scattering properties.

Of the many optical geometries possible for sensors, the use of evanescent fields in an optical waveguide appears to be the most advantageous for mass-producible microsensors. Evanescent field sensing localizes the optical field near a surface, ideal for discrimination between bound and unbound biochemical species in affinity assays, and is a natural approach when diode lasers are used as the light source. A representative evanescent field microsensor is shown in Fig. 1. This monolithically integrated device, called a tunable laser cavity sensor (TLCS) and developed in the DARPA BioFlips program, consists of a diode laser with an intracavity passive waveguide for evanescent field sensing [1]. A second diode laser, along with an optical field combiner and photodetector, are used as a heterodyne spectrum analyzer to sense optical frequency shifts due to binding of analytes to the sensing waveguide surface. The performance of this device was used to verify the analysis done within the work reported here.

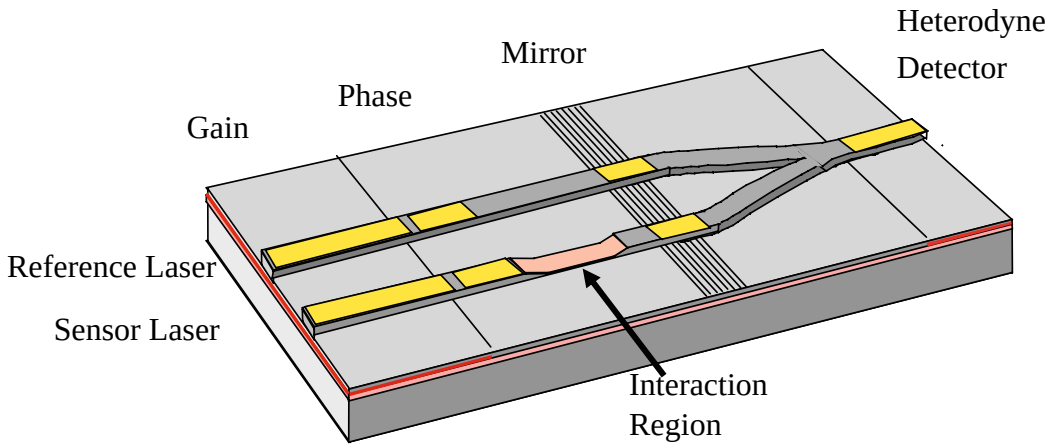

Figure 1. The tunable laser cavity sensor, representative of advanced biochemical microsensors. Changes in the refractive index at the surface of the interaction region induce a shift in the sensor laser's optical frequency, measured by heterodyne detection using an integrated reference laser.

2. Accomplishments

2.1 Molar Refraction and Index Increment

The index of refraction, or more frequently the index increment defined as the change in index of a solution due to a change in solute concentration, has long been used to identify or quantify proteins in solution. Indeed, most handbooks on biochemistry will contain a table of the index increments for many molecules. However, this data is generally measured at only one wavelength (the sodium D line, 589 nm), which is not a wavelength useful for microsensors since there are no integratable light sources operating at this wavelength. Measurements of the index increment at other wavelengths would provide useful dispersion data, and provide guidance on the most promising spectral range for advanced sensors.

The molar refraction R of a compound is related to the index of refraction by

$$R = \frac{\left(n^2 - 1\right)}{\left(n^2 + 2\right)} \frac{M}{d}, \qquad (1)$$

where n is the index of refraction (at wavelength λ), M is the molecular weight, and d is the density. It is known that the molar refraction of a molecule is approximately the sum of the contributions from the individual bonds, and that the index may be approximately predicted by summing the contributions from the molecule's structural components [2]. These molar refraction bond contributions have been tabulated, but only at 589 nm. We do not expect much variation from the 589 nm values for wavelengths from the visible into the near infrared, but there may be significant deviations for wavelengths in the ultraviolet or mid-infrared where strong absorptions occur. We thus undertook the task of determining spectrally resolved molar refraction values from the deep UV to the edge of the mid-IR.

The index of refraction is most commonly measured with an Abbe refractometer, but this instrument usually measures at a single wavelength, and can be used at other wavelengths only with difficulty. The second most common approach is to use surface plasmon resonance instruments, such as the Biacore, but these also have very limited spectral capabilities because the resonance can only be excited over narrow wavelength ranges. We have developed a new technique, utilizing Fabry Perot resonance in a custom spectrophotometer cell, to determine the index of refraction from the deep UV into the mid IR.

Fabry Perot resonance occurs when light undergoes multiple reflections within a cavity formed by two reflecting surfaces, as shown in Fig. 2. Whenever the round trip optical path length inside the cavity is a multiple of the wavelength of the light, the internal reflections add up in phase, and a maximum in the transmission (minimum in reflection) occurs. Since the optical path length is the product of the physical length and the index of refraction, if the path length is known, the transmission spectrum can be used to determine the index. The spectrophotometer cell consists of a pair of optical flats with dielectric mirror coatings. One flat has had a shallow recess etched into it. A few drops of sample fluid are placed in this well, and the mating flat is clamped across the top, forming a liquid-filled plane-parallel cavity. The assembly is then placed into a standard spectrophotometer, and the reflection spectrum is acquired.

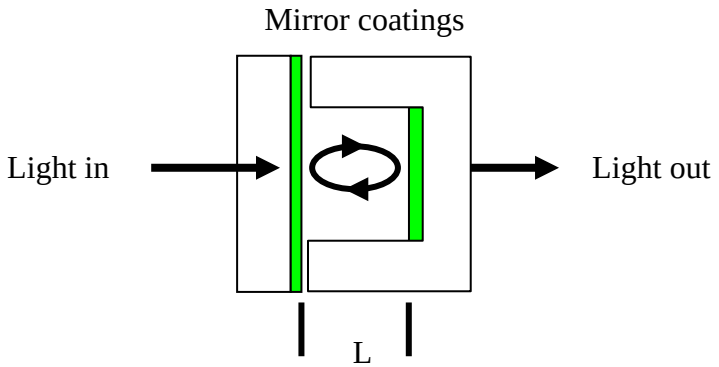

Figure 2. Schematic of the Fabry Perot resonator spectrophotometer cell.

Figure 3 shows the resulting reflection spectrum of methanol. The transmission peaks are clearly visible at the long-wavelength end, but are spaced too close together to see in this figure at the short-wavelength end. The envelope of the peaks and valleys is determined by absorption at short wavelengths, as well as the reflection spectrum of the dielectric mirror coatings.

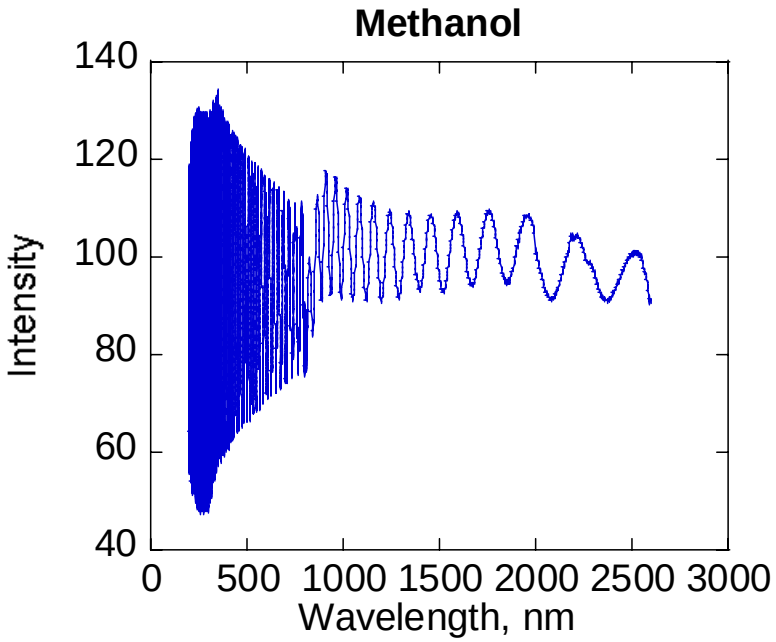

Figure 3. Reflection spectra of methanol from the deep UV to the mid-IR.

The reflection minima occur at $\lambda=2nL/m$, where L is the cavity length and m is the reflection fringe number, easily determined in the short cavity used here. Analysis of the spectra yields the index as a function of wavelength, from which the molar refraction $R(\lambda)$ may be determined.

To obtain $R(\lambda)$ for the basic structural components of biomolecules, we identified a set of reagents with similar structures, varying only one component. For example, by comparing methanol with ethanol and ethylene glycol, we can determine the contributions from the CH_3-, CH_2-, and OH- structural units. Fig. 4 shows the molar refraction for ten structural components important in amino acids, as a function of wavelength. For comparison, Fig. 5 shows the values evaluated at 589 nm, along with old literature values [2]. We find good agreement, validating our measurement technique.

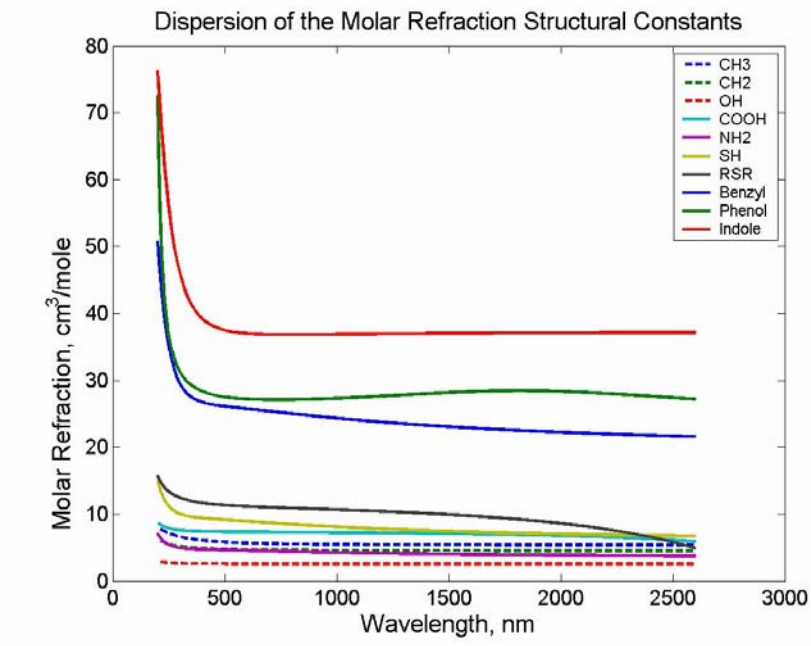

Figure 4. Molar refraction as a function of wavelength, for the structural components of the amino acids.

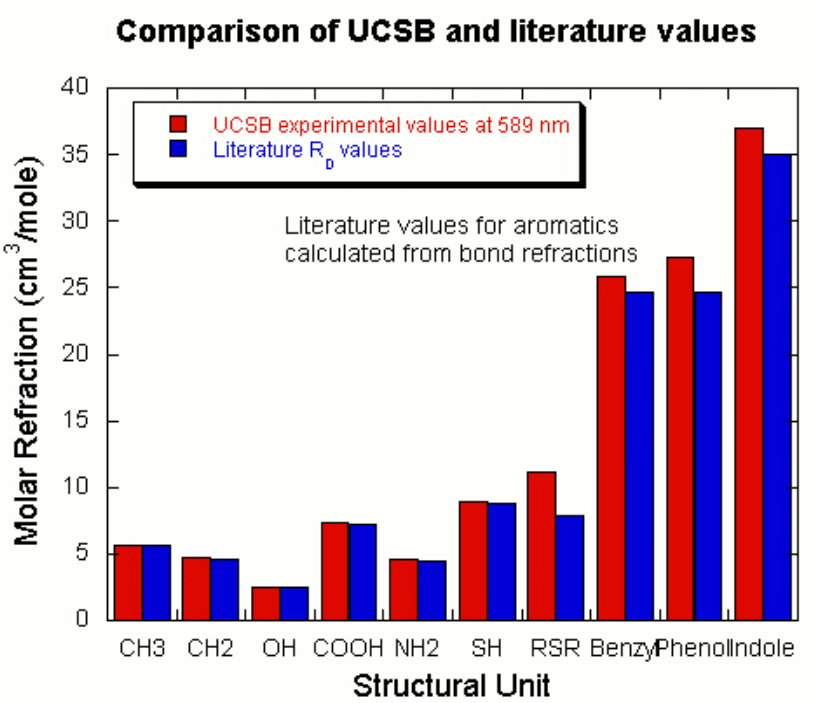

Figure 5. Comparison between the molar refraction values at 589 nm, and the literature values available only at 589 nm.

From these values, we can compute the molar refraction of the amino acids, as shown in Fig. 6. Since the amino acids are simple combinations of a few structural components, the dispersion curves are qualitatively similar to those in Fig. 3. We again get good agreement with literature values at 589 nm, but we now have data into the deep UV and mid-IR.

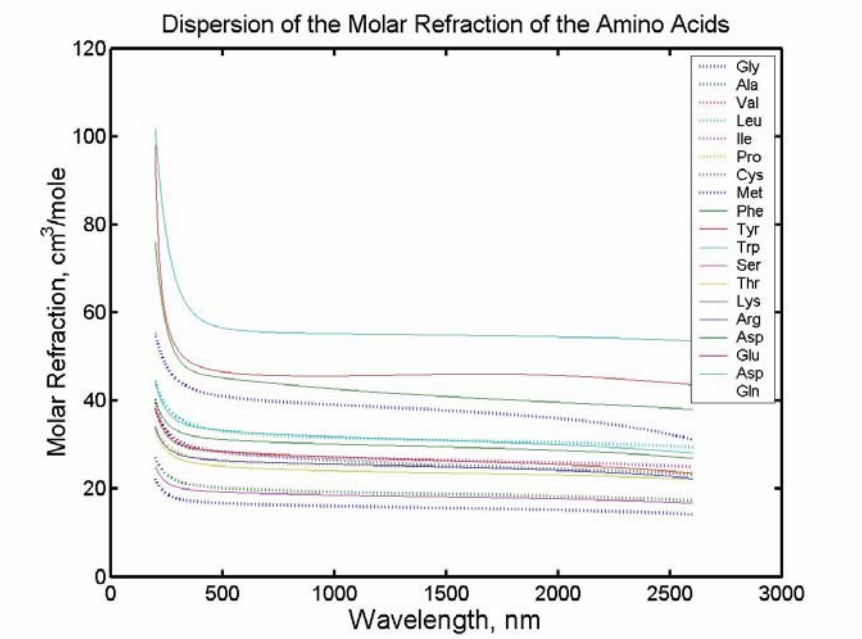

Figure 6. Molar refraction as a function of wavelength of the amino acids, calculated from the data in Fig. 4.

These results are not surprising: we expected strong dispersion in the UV, and little dispersion through the visible and NIR, though we could not previously quantify the dispersion. We thought that there might be significant dispersion beyond 2000 nm, due to absorption bands at 3200nm, but the effects are minimal except for tyrosine and methionine. A Kramers-Kronig analysis of published absorption spectra show that the mid-IR absorptions are too weak, and the photon energies are too low, to significantly impact the index below 3000 nm.

From the amino acid results, and using molecular weight and size data available from the protein data bank or other sources, we can calculate the molar refraction and hence index of refraction of arbitrary proteins. The calculated dispersion for the toxin Ricin is shown in Fig. 7. The strong dispersion below 400 nm might allow discrimination between similar proteins. For example, the calculated difference in index increment between trypsinogen and chymotrypsinogen is shown in Fig. 8. Measurement at wavelengths where the dispersion is low, for example at 1500 nm, could be used to quantify the amount of protein captured in an affinity assay, and subsequent measurement at 400 nm could be used to differentiate between similar proteins.

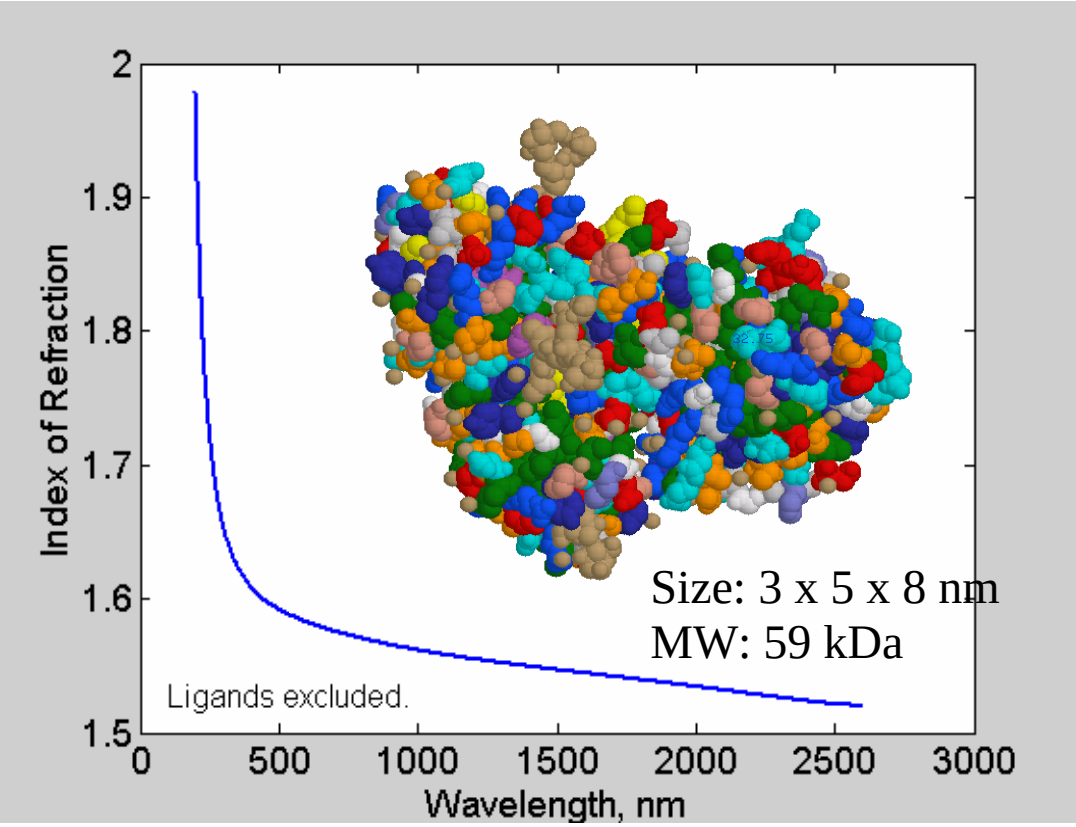

Figure 7. Calculated dispersion of the protein Ricin, based on amino acid content and density found from the Protein Data Bank. The amino acid residues are color-coded in the model.

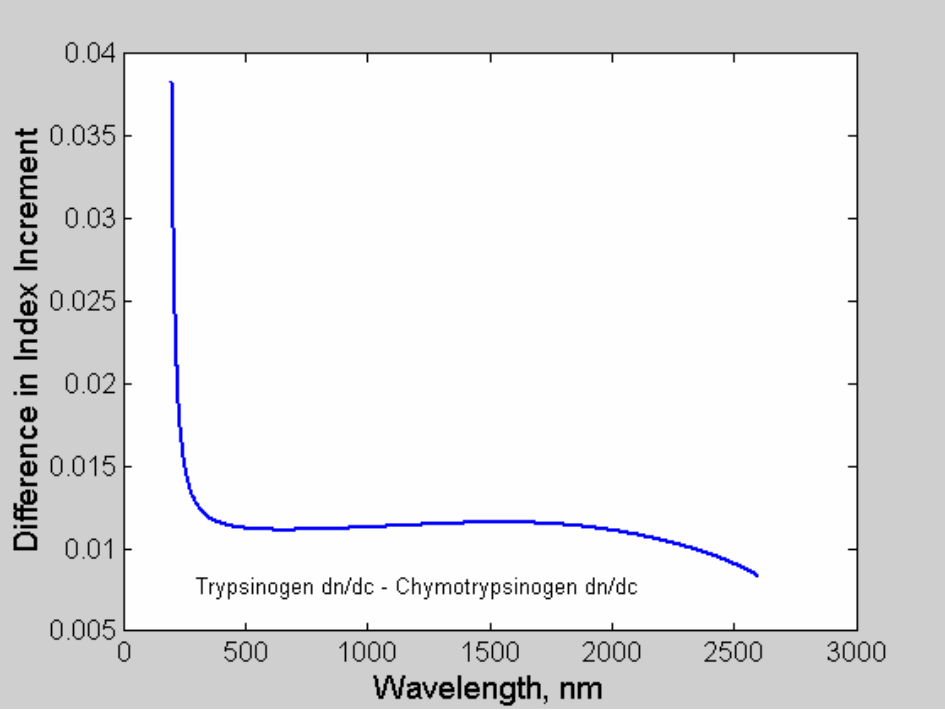

Figure 8. The calculated difference in index increment between the similar proteins trypsinogen and chymotrypsinogen. The strong dispersion below 400 nm might be used to differentiate between the two proteins.

2.2 Impact on Sensor Performance

2.2.1 Sensitivity

Evanescent field sensors rely on the penetration of the optical field out of a waveguide and into the analyte to be measured, and thus require a big overlap between the optical mode and the analyte to achieve high sensitivity. In Fig. 9(a), we show the calculated optical field profile in the ridge waveguide structure of the UCSB/Bioflips monolithic sensor. The only field penetration out of the waveguide occurs in the corners between the ridge and the waveguide layer, and the calculated mode overlap with all of the bulk fluid outside the waveguide is only 0.04%, in good agreement with experimental results [3]. The upper cladding cannot simply be thinned to increase the overlap, because the big difference between the waveguide index and the surrounding medium forces the optical

mode deep into the semiconductor. Indeed, as the upper cladding is thinned toward zero, the asymmetry cuts off propagation [4].

There is no cutoff of the lowest-order optical mode in a symmetrically clad waveguide. Thus, if we replace the lower cladding in the structure with a material of low index of refraction, approximately matching the index of refraction of the analyte, we should be able to thin the waveguide thickness and dramatically increase the mode overlap with the analyte. It has also been pointed out that to obtain high sensitivity to thin layers on the waveguide surface, such as used in affinity assays, a big difference between the core and cladding indices is needed, along with a thin core [5]. This was demonstrated with dielectric waveguides such as Si_3N_4/SiO_2 or TiO_2/SiO_2, which were considered high contrast with an index ratio of 2.2/1.5. In the case of semiconductor waveguides, even the "high" index dielectrics behave as low index cladding. In Fig. 9(b) we show the mode profile for a quasi-symmetrically clad channel waveguide formed between a GaInAsP core (n=3.452), a Si_3N_4 lower cladding (n=2.0), and an aqueous upper cladding (n=1.33). In comparison to Fig. 9(a), the mode profile is concentrated and symmetric, with significant energy in the evanescent field immediately next to the waveguide. In this case, the calculated mode overlap with a 10 nm thick antigen layer, bound to the top surface by a 10 nm thick antibody layer, is above 1%, two orders of magnitude greater than the original ridge waveguide design. We will assume such a quasi-symmetrically clad waveguide structure for the remaining sensitivity and scattering analysis.

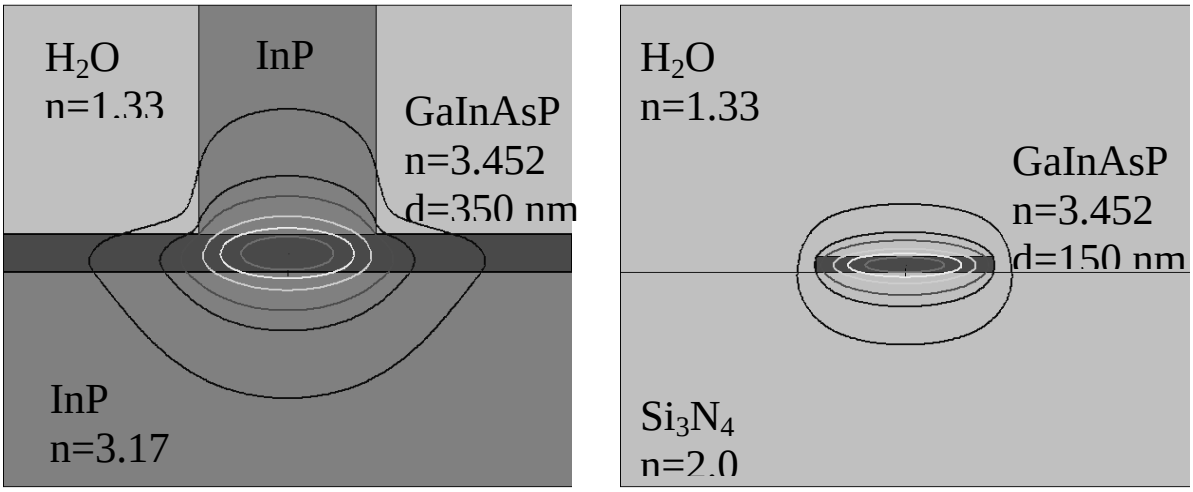

Figure 9. Optical mode profiles in the ridge waveguide used in the tunable laser cavity sensor, and in a quasi-symmetrically-clad channel waveguide.

To calculate the sensitivity of the sensor in the case of low-level detection, we need to know the shift in modal index due to binding of sparsely distributed particles of finite size. The change in refractive index of a fluid due to the uniform dispersion of N particles per unit volume is given by [6]

$$\Delta n = \frac{3}{2}\left(\frac{n'^2 - 1}{n'^2 + 2}\right)NV, \tag{2}$$

where n' is the ratio of the index of the particle to the index of the pure fluid, and V is the volume of the spherical particle. The product NV is just the fraction of space occupied by the particles. When the optical field is a waveguide mode, we must multiply by Γ_{xy} to account for limited overlap between the optical field and the particles. We also use the

mode volume, V_{mode}, to calculate N, noting that the mode confinement in the waveguide core, $V_{mode} = V_{core} / \Gamma_{core}$:

$$N = N^{\#} \frac{\Gamma_{core}}{V_{core}}, \tag{3}$$

where $N^{\#}$ is the number of particles on the surface (a pure number). For particles of radius a, we estimate the mode overlap Γ_{xy} by calculating the optical intensity at the center of the particle and multiplying by the particle area. This is equivalent to assuming that the evanescent field decay is approximately linear over the dimension of the particle. Then,

$$\Delta n = \frac{3}{2}\left(\frac{n'^2 - 1}{n'^2 + 2}\right)\Gamma_{xy} N^{\#} \frac{\Gamma_{core}}{V_{core}}\left(\frac{4}{3}\pi a^3\right). \tag{4}$$

In Fig. 10, we show the change in modal index as a function of the number of particles bound to a waveguide of dimensions 0.15 μm x 2 μm x 1000 μm. We use the particle radius as a second parameter, assume the particle index of refraction is 1.57 representative of polystyrene nanoparticles (and approximately correct for proteins) and assume that the surrounding medium is water with index 1.33. The curves terminate at the close-packed number given by (waveguide length x waveguide width) / (particle diameter^2).

Also shown in Fig.10 is the theoretical sensitivity limit of the tunable laser cavity sensor. We see that for protein antigens 5 nm in radius, $2 \cdot 10^5$ copies must be bound. This corresponds to about 150 femtograms of material. For macromolecules or pathogens larger than 50 nm in radius, single copies should be detectable.

A number of researchers have used polystyrene beads bound to the target antigens to enhance the sensitivity of refractometric measurements [7]. This is particularly useful when the target is a small molecule such as a drug. A thousand-fold improvement in sensitivity has been reported, easily understood by reference to Fig. 10. If the low index polystyrene is replaced by a high index semiconductor nanoparticle such as silicon, (2) shows that the sensitivity may be further improved by a factor of five.

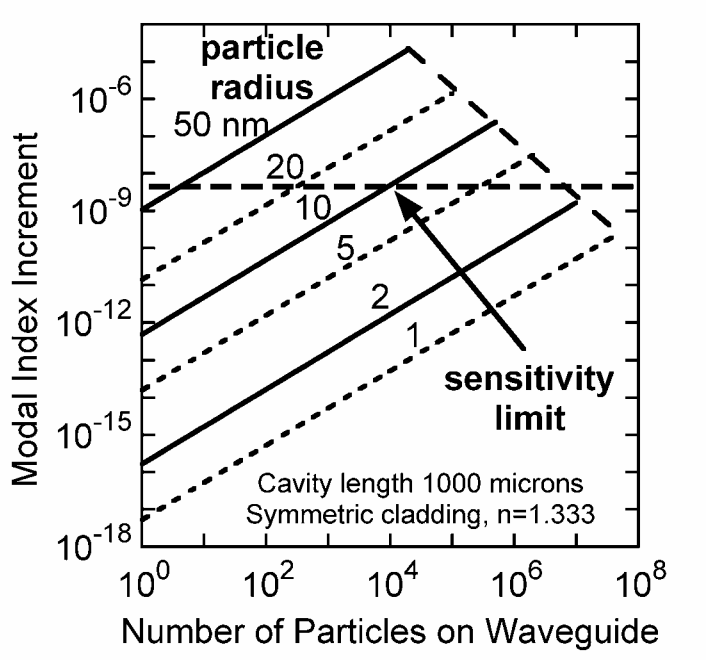

Figure 10. Modal index increment as a function of the number of particles on the sensing waveguide.

2.2.2 Scattering and Absorption

If the mode overlap with particles on the waveguide surface is made large, the sensor might also suffer a significant increase in optical scattering loss. To evaluate this potential problem, we adapt Rayleigh scattering theory [6]. The scattering cross section

C_{sca} is the total power scattered by a particle *dP*, normalized by the incident intensity at the particle:

$$C_{sca} = dP \Big/ \left(\Gamma_{xy} P_0 \Big/ \pi a^2 \right). \tag{5}$$

Let N_A be the surface density of identical particles on the waveguide of width *w*. Upon traversing length *dz*, the optical field will suffer a loss

$$\frac{dP}{P_0} = -N_A w dz \Gamma_{xy} \frac{C_{sca}}{\pi a^2}. \tag{6}$$

Rearranging to obtain an expression for *dP/dz*, and solving the differential equation yields

$$P(z) = P_0 \exp\left[- N_A w \Gamma_{xy} \frac{C_{sca}}{\pi a^2} z \right]. \tag{7}$$

Inserting the scattering cross section of a small spherical particle ($a << \lambda$) [6] and identifying the exponential decay term as the modal loss $\langle \alpha \rangle$, we arrive at

$$\langle \alpha \rangle = -N_A w \Gamma_{xy} \frac{128}{3} \pi^4 \left(\frac{a}{\lambda} \right)^4 \left(\frac{n'^2 - 1}{n'^2 + 2} \right)^2. \tag{8}$$

The dependence on $(a/\lambda)^4$ limits the scattering loss in the tunable laser cavity sensor, which operates at 1550 nm. Indeed, for proteins or polystyrene particles, the loss remains below 1 cm^{-1} even up to the close-packed surface density. Note that the dependence on the relative index is stronger for scattering than for the index increment. If high-index particles are used for sensitivity enhancement, the scattering loss increases faster. Nonetheless, even for silicon particles the scattering doesn't become significant until the

particle radius exceeds 20 nm and the particle density approaches the close packed limit, as Fig. 11 shows. We point out that Rayleigh scattering assumes that the particles are sufficiently isolated so that phase coherence between scatterers may be ignored. This is clearly not valid in the close-packed limit, at which point a coupled-mode analysis may be more appropriate. In any case, the only instance relevant to sensing in which the scattering may be a problem is for a nanoparticle-enhanced flow assay, in which the enhancing particles are packed closely on the waveguide, and released upon binding of an untagged antigen.

We might also ask whether the increased field penetration out of the sensing waveguide can lead to significant absorption loss. In most chemical or biological materials, the absorption in the near infrared region is dominated by overtones of the mid-infrared absorption bands of C-H, O-H and N-H bonds [8]. These overtones are weak, even in pure materials. In fact water, the most likely solvent for biochemical sensing, has stronger absorption than organics, amounting to A = 3.2 through a 1 cm path length. This corresponds to a loss α = 7.4 cm^{-1}. NIR absorption in alkanes is roughly half this value. Even if $\Gamma_{xy}\Gamma_z$ = 10^{-2}, as in the case of a TLCS with a symmetrically clad sensing waveguide, the additional modal loss seen by the laser is less than 0.1 cm^{-1}. Proteins, and the alkane linker molecules commonly used to immobilize antibodies or nucleotides to surfaces also contain these absorbing bonds, but always at a lower density than in the pure solvents. We conclude that absorption loss will not be significant. One possible exception is if semiconducting nanoparticles or quantum dots are used for assay enhancement. In this case, the absorption edge of nanoparticle can be engineered to be remote from the sensor wavelength.

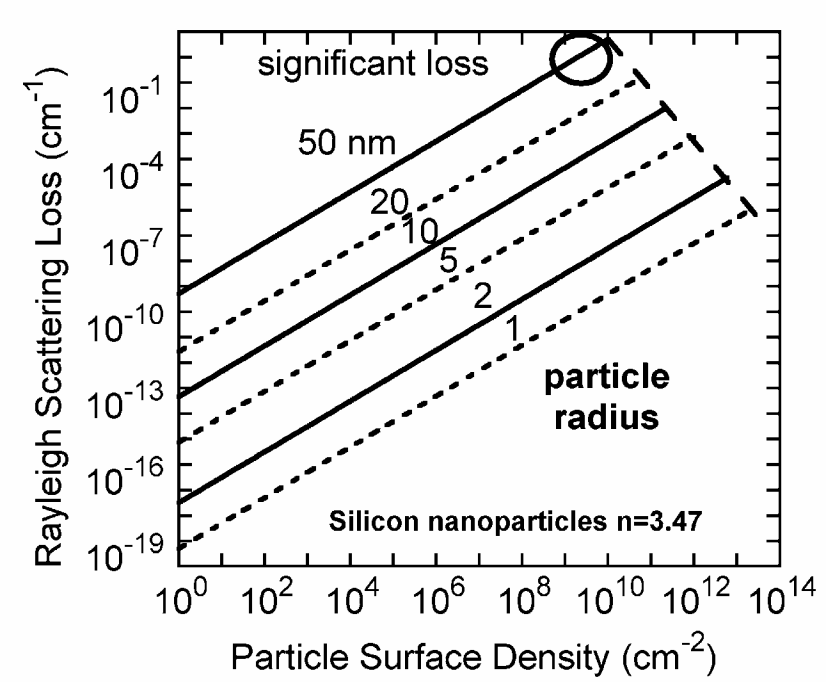

Figure 11. Scattering loss from high-index particles on the waveguide surface. Loss only becomes significant near the close-packed surface density. For proteins or latex particles, the scattering loss is insignificant.

2.3 Monolithic Particle Sensor

The results above, regarding low scattering from particles on a waveguide, are based on the Rayleigh assumption that the particles are much smaller than the wavelength of the scattered light. For larger particles, the scattering can become significant. This was verified using another sensor developed in the BioFlips project, one that implemented the channel waveguide structure discussed previously to obtain higher sensitivity [9]. The scattering results suggest that the device might be useful as a spore sensor or cell cytometer.

The diode laser sensor used for these experiments is shown schematically in Fig. 12. The key innovation is a sensing waveguide formed by wet oxidation of an $Al_{0.98}Ga_{0.02}As$ layer beneath an $Al_{0.2}Ga_{0.8}As$ waveguide layer. The oxide index of refraction is approximately 1.6, fairly close to that of both water and protein, whereas the semiconductor waveguide index is 3.4. The large and nearly symmetric difference

between the core index and the cladding index allows a large overlap between the optical field propagating along the waveguide and the material immediately adjacent to the waveguide. This provides a hundred-fold improvement in the sensitivity of the biosensor, but may also lead to scattering loss from species larger than 100 nm in diameter. We measured this directly by lowering a dielectric probe, approximately 1.5 μm in diameter, directly onto the waveguide, while simultaneously measuring the laser optical power and wavelength. A piezoelectric element was used to control the probe position. The synchronously detected power loss amounted to about 6% of the total power. A numerical model predicts that about 4% of the optical power penetrates out of the waveguide into the sensing region, so our measurement indicates that the dielectric probe scatters *all* of this light out of the lasing mode.

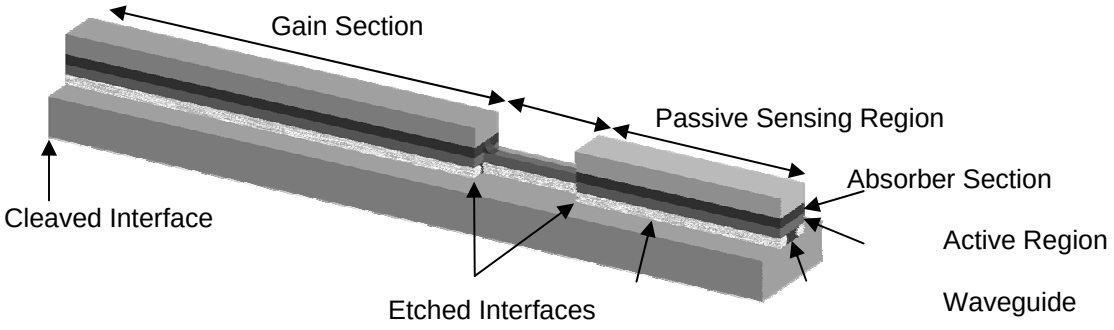

Figure 12. Schematic of the coupled cavity laser sensor. Note the narrower ridge width in the sensing region, allowing complete oxidation beneath the waveguide layer to form a quasi-symmetrically clad waveguide.

One implication of this result is that the since the light that interacts with the large particle is lost from the cavity, the phase delay produced by the particle does not show up as a shift in the cavity resonance. This means that sensors such as waveguide interferometers or the Bioflips heterodyne sensor will be significantly less sensitive to large particles than would be predicted if scattering is ignored.

On the other hand, this small cavity loss can be used in its own right to detect spores or cells. We demonstrated a monolithic particle detector by reverse biasing the absorber section shown in Fig. 12, and using it as an integrated photodetector. A nanoliter drop of water containing about one thousand 1 μm diameter latex spheres was placed on the sensing region. The reflectivity at the etched facet between the gain and sensing regions was lowered by the presence of water, and so the laser's threshold current increased and the output power at fixed current decreased, as shown in Fig. 13. After 15 seconds, the water evaporated, and the signal increased again, but not quite to the original level. Photomicrographs of the sensing region revealed that a cluster of particles landed on the waveguide when the water evaporated, leading to a scattering loss in the compound cavity and causing the reduced power at the detector. Such a cluster is similar in size to a cluster of Anthrax spores. The sensitivity was high enough to detect single 1 μm latex particles. Such intracavity detection has been reported before, using external cavity lasers, but we are not aware of any prior demonstration in a robust and low cost monolithic format.

3. Summary

The formalism of molar refraction was extended to cover the wavelength range of 200 nm - 2500 nm, in order to predict the index of refraction and index increment of a wide range of molecules of biochemical interest. Data for the model was obtained using a unique interferometer cell within a standard laboratory spectrophotometer. The resulting models for protein index increment suggest that both the sensitivity and specificity of refractometric sensors may be improved by operating at ultraviolet wavelengths, and that measurement at two wavelengths may be used to quantify the total

protein present and distinguish between similar proteins, of potential use to reduce false positive responses in affinity assays.

The impact of refractive index and particle size on semiconductor-based evanescent field sensors was analyzed, along with the magnitude of optical scattering. The results are particularly important in quantitatively explaining the benefits of using a nanoparticle-enhanced assay, and of using high-index nanoparticles for enhancement. For particles below 100 nm in diameter, optical scattering will be negligible. For particles larger than 100 nm, scattering becomes measurable, and single 1 μm diameter particles were detected in a novel monolithic evanescent field sensor.

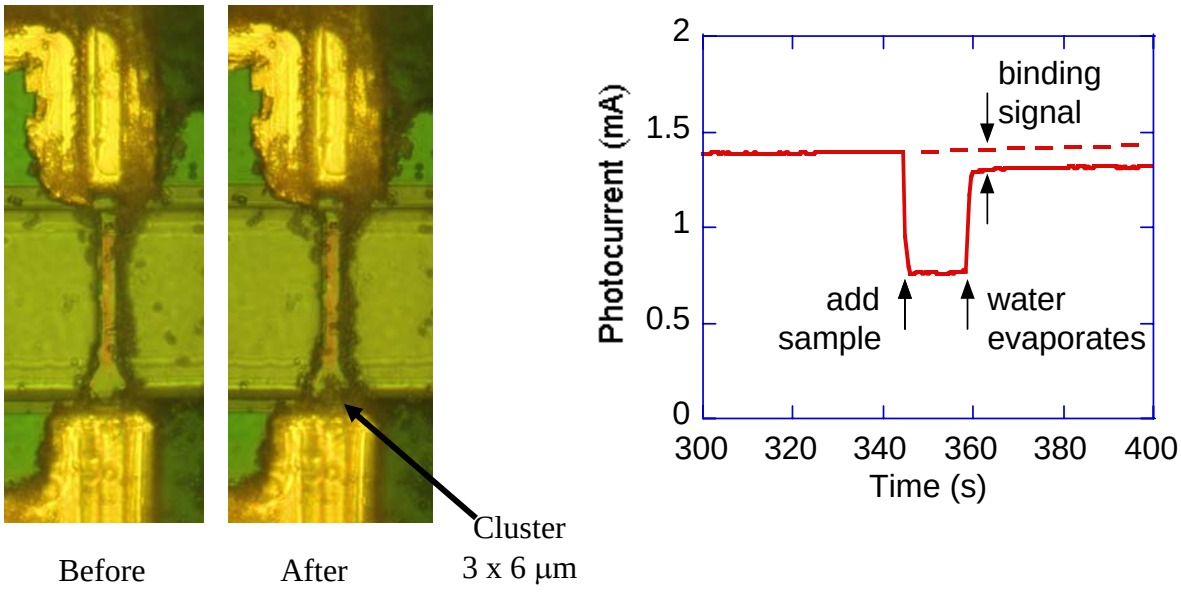

Figure 13. Particle sensing with the coupled cavity laser sensor. A nanoliter droplet of water containing 1 μm diameter latex spheres is placed on the sensing waveguide and allowed to evaporate, leaving behind spheres or small clusters of spheres. The difference in photocurrent measured at the absorber indicates the presence of particles, seen in this case to be a single cluster similar in size to a cluster of anthrax spores.

4. References

[1] D. A. Cohen, E. J. Skogen, H. Marchand, and L. A. Coldren, "Monolithic chemical sensor using heterodyned sampled grating DBR lasers," *Electronics Letters*, vol. 37, pp. 1358-1360, 2001.

[2] T. L. McMeekin, M. L. Groves, N. J. Hipp, "Refractive indices of amino acids, proteins, and related substances, in Amino Acids and Serum Proteins, Advances in Chemistry Series #44, American Chemical Society, 1964.

[3] D. A. Cohen, J. Nolde, A. Tauke Pedretti, C. S. Wang, E. J. Skogen, L. A. Coldren, "Sensitivity and scattering in a monolithic heterodyned laser biochemical sensor," accepted for publication in *IEEE J. Special Topics in Quantum Electronics*, 2003.

[4] L. A. Coldren and S. W. Corzine, *Diode Lasers and Photonic Integrated Circuits*. New York: John Wiley and Sons, 1995, appendix 3.

[5] O. Parriaux and G. J. Veldhuis, "Normalized analysis for the sensitivity optimization of integrated optical evanescent-wave sensors," *Journal of Lightwave Technology*, vol. 16, pp. 573-582, 1998.

[6] M. Kerker, *The Scattering of Light*. New York: Academic Press, 1969, ch. 3.

[7] S. Kubitschko, J. Spinke, T. Bruckner, S. Pohl, and N. Oranth, "Sensitivity enhancement of optical immunosensors with nanoparticles," *Analytical Biochemistry*, vol. 253, pp. 112-122, 1997.

[8] B. Osborne, "Near infrared spectroscopy in food analysis," in *Encyclopedia of Analytical Chemistry*, vol. 5, R. A. Meyers, Ed., New York: John Wiley and Sons, 2000, pp. 4069-4082.

[9] C. S. Wang, D. A. Cohen, J. A. Nolde, D. D. Lofgreen, L. A. Coldren, "A diode laser chemical sensor utilizing an oxidized lower cladding layer for high sensitivity", presented at the IEEE LEOS Annual Meeting, Tucson AZ, Nov 2003.

5. Publications, Conference Presentations

D. A. Cohen, J. Nolde, A. Tauke Pedretti, C. S. Wang, E. J. Skogen, L. A. Coldren, Sensitivity and scattering in a monolithic heterodyned laser biochemical sensor *IEEE J. Special Topics in Quantum Electronics*, Vol. 9, September/October 2003.

C. S. Wang, J. A Nolde, D. D. Lofgreen, L. A. Coldren, D. A. Cohen, "A self-aligned process to monolithically integrate a quasi-symmetrical sensing waveguide to a diode laser chemical sensor", submitted to *Applied Physics Letters*, 2003.

Sensitivity and scattering in an integrated heterodyned laser biochemical sensor
Cohen, D. A.; Skogen, E. J.; Nolde, J.; Coldren, L. A.;
Semiconductor Laser Conference, 2002. IEEE 18th International, 29 Sept.-3 Oct. 2002
Pages: 29-30.

6. Personnel

Dr. Daniel A. Cohen, Principal Investigator
Ms. Danielle Turner, student assistant
Ms. Sarah Delaney, student assistant
Ms. Amy Bourgeois, student assistant